Fibrin Selective Alteplase with Improved Thrombolysis and Inhibition Resistance Engineered by Rational Design

Toul M.[1,2,#], Slonkova V.[1,#], Mican J.[1,2,#], Thalerova S.[2,3], Peskova M.[2,3,4], Kittova P.[2,4,5], Scheer P.[2,6], Hlozkova J.[2,6], Brhelova E.[2,7], Aksu D.A.[2,6], Biskupic J.[2,7], Ondrus J.[2,8], Kasparek P.[9], Batkova T.[2,9,10], Marek M.[1,2], Vitecek J.[2,3], Kubala L.[2,3], Mikulik R.[2,10], Damborsky J.[1,2], Bednar D.[1,2,*], Prokop Z.[1,2,*]

1. Loschmidt Laboratories, Department of Experimental Biology and RECETOX, Faculty of Science, Masaryk University, Kamenice 5/C13, 625 00 Brno, Czech Republic
2. International Clinical Research Center, St. Anne's University Hospital, Pekarska 53, 656 91 Brno, Czech Republic
3. Department of Biophysics of Immune System, Institute of Biophysics of the Czech Academy of Sciences, Kralovopolska 135, 612 65 Brno, Czech Republic
4. Department of Biochemistry, Faculty of Science, Masaryk University, Kamenice 5, 625 00 Brno, Czech Republic
5. Department of Biochemistry, Faculty of Medicine, Masaryk University, Kamenice 5, 625 00 Brno, Czech Republic
6. Department of Pharmacology and Toxicology, Faculty of Pharmacy, Masaryk University, Palackeho trida 1946/1, 612 00 Brno, Czech Republic
7. Department of Chemical Drugs, Faculty of Pharmacy, Masaryk University, Palackeho trida 1946/1, 612 00 Brno, Czech Republic
8. Veterinary Research Institute, Hudcova 296/70, 621 00 Brno, Czech Republic
9. BioVendor LM, Karasek 1767/1, 621 00 Brno, Czech Republic
10. Department of Neurology, Tomas Bata Regional Hospital, Havlickovo nabrezi 600, 762 75 Zlin, Czech Republic

[#] These authors contributed equally to the work

* Corresponding authors

Abstract

AIMS: Thrombolytic enzymes represent an accessible and streamlined treatment for acute ischemic stroke, yet current FDA-approved agents, alteplase and tenecteplase, are limited by incomplete recanalization, hemorrhagic risk, and neurotoxicity. We aimed to develop a multidisciplinary workflow for rational design and multi-level testing of thrombolytic proteins to generate a next-generation thrombolytic with improved potency and safety.

METHODS AND RESULTS: Our pipeline integrated *in silico* design, biochemical characterization, *in vitro* thrombolysis, and *in vivo* validation. Computational screening included rational mutagenesis to reduce side effects, reconstructed ancestral sequences, and database-mined homologs. Selected candidates were biochemically assessed for enzymatic activity, fibrin stimulation, selectivity and affinity, inhibition resistance, and clot penetrability. The most promising variants underwent *in vitro* clot thrombolysis and *in vivo* efficacy and safety studies in rats. Brnoteplase emerged as the lead candidate, exhibiting 80-fold enhanced fibrin selectivity, 4-fold higher inhibition resistance, and superior clot penetrability compared to alteplase. *In vitro*, Brnoteplase demonstrated deeper intrathrombus penetration and a progressive dose–response profile, unlike alteplase, which declined at higher concentrations. *In vivo*, Brnoteplase achieved higher thrombolysis rates and recanalization frequency across all doses, with extended biological half-life enabling bolus administration. Safety assessments revealed the lowest incidence of severe hemorrhagic transformation and minimal hemispheric asymmetry.

CONCLUSIONS: We established a robust pipeline for efficient generation and selection of novel thrombolytics and identified Brnoteplase as a promising candidate combining improved fibrin selectivity, inhibition resistance, biological half-life, and clot penetration. These features translate into higher thrombolytic efficacy and a promising safety profile *in vivo*, warranting further preclinical evaluation to confirm its potential as a next-generation thrombolytic for acute ischemic stroke.

Introduction

Cardiovascular diseases, including ischemic stroke, represent the leading cause of morbidity and mortality worldwide, and the burden continues to rise[1]. Ischemic stroke therapy based on mechanical thrombectomy is restricted to specialized stroke centers and will therefore never become a universal solution[2]. In contrast, drug-induced thrombolysis treatment is readily accessible, more affordable, and straightforward to administer, so it remains the first-line, widely applicable therapy[3]. Unfortunately, current thrombolytic drugs still possess major limitations[4] and their further improvement is critical to reverse the alarming statistics and growing socioeconomic burden of stroke[5].

For almost 30 years, alteplase was the only Food and Drug Administration (FDA)-approved thrombolytic drug for acute ischemic stroke. Despite its proven effectiveness, it exhibits several drawbacks, including lower than 50 % recanalization rates, short half-life, and an increased risk of intracranial hemorrhage[6,7]. In March 2025, tenecteplase was approved by the FDA as the second drug for acute ischemic stroke treatment[8]. Tenecteplase is a mutant variant of alteplase with higher fibrin specificity and improved inhibition resistance, resulting in an extended half-life that enables bolus administration[9]. However, tenecteplase does not show clear superiority over alteplase in terms of efficacy or safety[10-13]. Therefore, there is a continuous need to develop a more efficient and safer thrombolytic drug with attenuated side effects.

An ideal thrombolytic should be not only more active but primarily more fibrin-selective and with alleviated binding to receptors, namely low density lipoprotein receptor-related protein 1 (LRP1) and N-methyl-D-aspartate receptor (NMDAR)[14]. These properties would make the thrombolytic safer by decreasing hemorrhagic and neurotoxicity risks[15,16]. Furthermore, reduced receptor binding combined with enhanced plasminogen activator inhibitor-1 (PAI-1) resistance would prolong the agent biological half-life, increasing overall efficacy throughout the therapeutic window and allowing convenient bolus administration, as achieved with tenecteplase[17].

Here, we report the development of an experimental pipeline for the design, comprehensive characterization, and selection of novel thrombolytic drugs (**Figure 1**). The pipeline allows for

initial screening of numerous candidate thrombolytics and their systematic filtering at multiple levels to select only the most promising variants for demanding and ethically sensitive *in vivo* animal and preclinical studies. We validated the robustness of this pipeline by generating improved variants of current thrombolytics based on plasminogen activation. The final selection resulted in an alteplase variant, denoted Brnoteplase, which exhibited favorable therapeutic properties, making it a promising candidate for clinical studies and a valuable starting point for follow-up improvements.

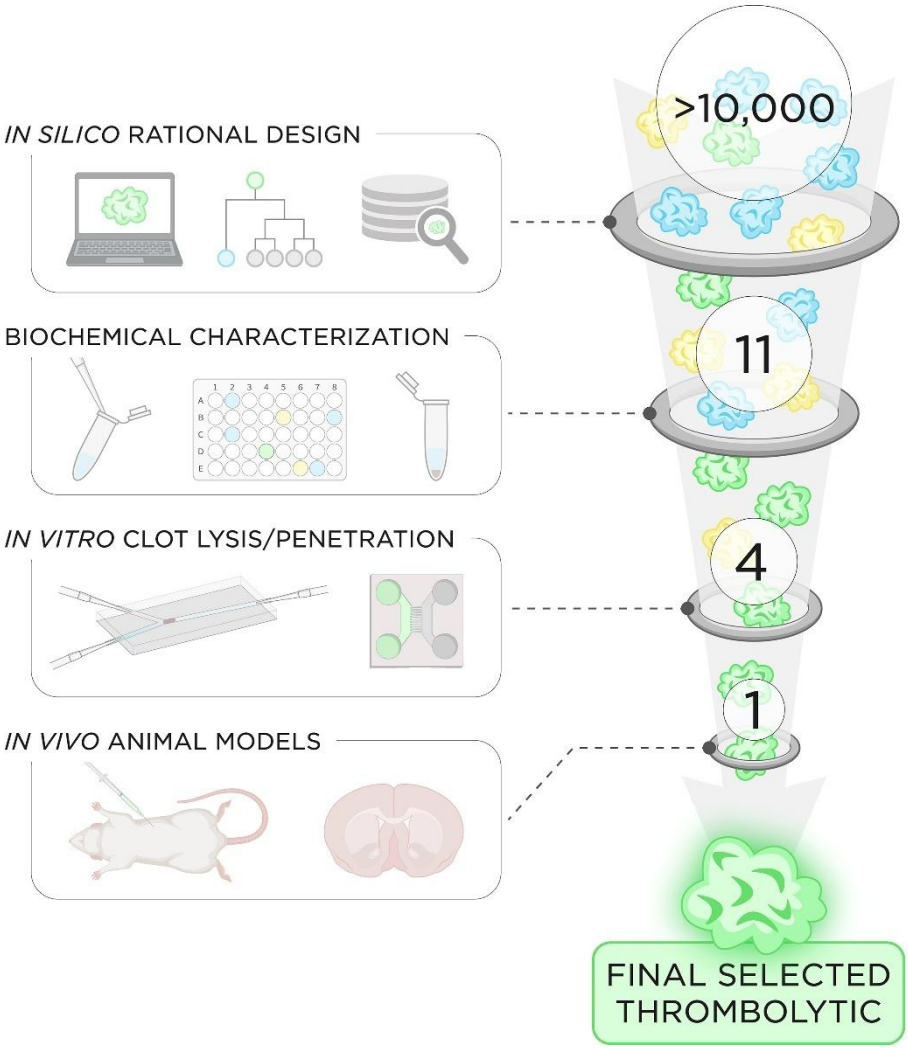

Figure 1: Schematic illustration of the research workflow established in this study to develop a novel improved thrombolytic. The pipeline involves (i) *in silico* rational design of new thrombolytic protein sequences, (ii) their biochemical characterization, (iii) testing in *in vitro* thrombolysis and penetration assays, and (iv) validation in *in vivo* animal rat models. The numbers in the circles correspond to the number of thrombolytic protein variants advanced to each step (grey rings) of the workflow, enabling initial screening of more than 10,000 variants and their comprehensive filtering down to one selected thrombolytic to be verified in resource-demanding preclinical *in vivo* models.

93 # Methods

94 **Computer-aided selection of mutations alleviating binding of tPA to LRP1**

95 Computational design of alteplase variants with reduced binding to the LRP1 receptor was
96 performed using (i) structure-based and (ii) sequence-based strategies.

97 In the structure-based strategy, we performed conservation and correlation analysis of lysine
98 residues on the first four domains of alteplase, which are responsible for LRP1 binding, using the
99 HotSpot Wizard web server[18]. Afterwards, we docked the structure of LRP1 complement-like
100 binding repeat to tissue-type plasminogen activator (tPA) using ClusPro and RosettaDock[19]. We
101 clustered the docked structures and evaluated distances of conserved and exposed lysines of tPA
102 to the lysine-binding site of LRP1. Lastly, we have performed molecular dynamics (MD) of tPA
103 and evaluated which pairs of lysines are in the required distance of 21 to 29 Å for binding LRP1[20].
104 We designed mutant tPAs lacking specific lysines. These lysines fulfil the following criteria: (i)
105 conserved in homologous sequences, (ii) exposed on the protein surface, (iii) located on the first
106 four domains of tPA responsible for LRP1 binding, (iv) located on the interface with LRP1
107 complement-binding repeat in cluster centres of docked structures, and (v) being within 21 – 29
108 Å of another lysine residue in tPA during MD simulations.

109 In the sequence-based strategy, we compared the tPA sequence to its homolog, desmoteplase,
110 which competitively binds LRP1[21]. In the pairwise sequence alignment, we identified lysines in
111 both tPA and desmoteplase at homologous positions. These lysines are likely candidates to
112 mediate LRP1 binding.

113 Lysine positions identified by structure- and sequence-based strategies were subjected to *in*
114 *silico* saturation mutagenesis using the Rosetta ddg_monomer application. Mutated residues that
115 retained thermodynamical stability were selected for experimental characterization.

116 **Combining beneficial tPA mutations from literature:**

117 To identify mutations for enhancing the efficacy and safety of tPA, we performed
118 a comprehensive literature review on the structural biology and protein engineering

119 of thrombolytics. We then sought an innovative combination of mutations to improve tPA's
120 efficacy and safety and combined them into a multiple mutant for experimental
121 characterization.

122 **Ancestral sequence reconstruction of tPA-related proteins**

123 The sequence of tPA, including the signal peptide, was submitted to the FireProt^{ASR} web server[22].
124 The calculation was performed using default settings. Ancestral sequences for experimental
125 characterization were selected using the following criteria: (i) as few insertions or deletions
126 compared to tPA as possible, (ii) preserved catalytic residues, and (iii) preserved functionally
127 important residues known to influence different tPA functions.

128 **Mining novel enzymes from sequence databases**

129 EnzymeMiner was used to search for novel thrombolytic enzymes in protein sequence
130 databases[23]. Two separate runs were performed using tPA and desmoteplase as query sequences.
131 Proteins with transmembrane regions or mutated catalytic residues were discarded. Moreover,
132 proteins had to contain key domains for plasminogen activation and fibrin binding and score a
133 predicted solubility higher than the query sequence. After filtering for these characteristics,
134 proteins with interesting properties were selected manually.

135 **Construction of mutant gene sequences**

136 For each designed thrombolytic variant, a synthetic gene (Genscript) was cloned into the
137 expression vector pcDNA3.1 (Thermo Fisher Scientific). *E. coli* strain TOP10F (Thermo Fisher
138 Scientific) was transformed with the plasmid construct. Plasmid DNA was isolated for transient
139 transfection using Plasmid Giga Kit (Qiagen).

140 **Heterologous gene expression and protein isolation**

141 HEK-293E cells were adapted to suspension growth in HyClone™ CDM4HEK293 serum-free medium
142 (Cytiva) supplemented with 4 mM L-glutamine (AppliChem). Prior to transient transfection, HEK-
143 293E cells were centrifuged at 250 g for 10 minutes and resuspended at the density of $2x10^7$
144 cells/ml in the Gibco™ FreeStyle™ 293 expression medium (Thermo Fisher Scientific). HEK-293E

145 cells were transiently transfected by plasmid DNA and linear 25-kDa polyethyleneimine
146 (Polysciences) at a 1:2 ratio and a final concentration of 25 and 50 ug/mL, respectively. Plasmid
147 pmaxGFP at 5 % of the total DNA content was added as a positive control of the transfection
148 process. Four hours after transfection, cells were diluted with HyClone medium containing 2 mM
149 L-glutamine. The cells were cultured at 37 °C and 130 rpm in an incubator shaker (New Brunswick
150 Innova® 44/44R). The culture supernatants were harvested 7 days post-transfection. The
151 supernatant was purified on Ni-NTA column (Protino, Macherey-Nagel) connected to the BioLogic
152 DuoFlow FPLC system (Bio-Rad) and equilibrated with the purification buffer (10 mM Tris-HCl pH
153 7.5, 200 mM NaCl). The thrombolytic protein bound to the column was washed and eluted with
154 10 mM and 250 mM imidazole in buffer 10 mM Tris-HCl buffer pH 7.5 with 200 mM NaCl and 200
155 mM L-Arginine. Subsequently, the protein was purified on the Superose 6 SEC column (GE
156 Healthcare) equilibrated with PBS buffer pH 7.4, 200 mM L-Arginine. The protein was
157 supplemented with 0.01 % of Tween 80 and stored at 4 °C.

158 **Protein thermostability measurement**

159 Protein thermostability was determined by analyzing changes in protein intrinsic tryptophan
160 fluorescence with increasing temperature using the nanoscale differential scanning fluorimetry
161 (nanoDSF) instrument Prometheus NT.48 (NanoTemper Technologies). Each measurement was
162 performed in triplicate in phosphate-buffered saline PBS pH 7.4 (10 mM Na_2HPO_4, 1.8 mM KH_2PO_4,
163 2.7 mM KCl, 137 mM NaCl) containing 3.5 % L-arginine, and 0.01 % Tween 80. The fluorescence
164 was monitored at temperatures ranging from 20 °C to 100 °C with a temperature ramp of 1
165 $°C.min^{-1}$ and the values of the fluorescence ratio at 350/330 nm were plotted against
166 temperature. The values of onset temperature (T_{onset}) and melting temperature (T_m) were
167 determined using the manufacturer-provided software after deriving the obtained fluorescence
168 curves. The final values were expressed as averages of individual replicates and their respective
169 standard deviations.

170

171

172 **Determination of enzymatic activity and fibrin(ogen) stimulation and selectivity**

173 The activities of thrombolytic enzymes were measured using the fluorogenic substrate D-VLK-
174 AMC (AAT Bioquest), which is converted by the generated plasmin molecules to the fluorescent
175 product 7-amino-4-methylcoumarin (AMC), whose fluorescence was monitored. All the
176 experiments were performed at 37 °C in phosphate-buffered saline PBS pH 7.4 (10 mM Na_2HPO_4,
177 1.8 mM KH_2PO_4, 2.7 mM KCl, 137 mM NaCl) containing 1 mM $CaCl_2$, 0.0035 % L-arginine, and 0.01
178 % Tween 80 and each measurement was repeated in three replicates. The activities were
179 determined in the absence but also in the presence of fibrinogen or fibrin that served as
180 stimulation agents. In the case of fibrin stimulation, small fibrin clots were formed in a
181 microplate well of a black clear bottom 96-well plate by mixing 8 µL of human fibrinogen
182 (HYPHEN BioMed) with 2 µL of human thrombin (Sigma-Aldrich). The wells were sealed with an
183 adhesive foil to prevent evaporation and kept at room temperature for an hour to ensure
184 complete polymerization and clot formation. In the case of fibrinogen stimulation, the
185 microplate wells were filled with 8 µL of human fibrinogen mixed with 2 µL of the reaction buffer
186 only. In the absence of any stimulant, only 10 µL of the reaction buffer was injected. After that,
187 all the microplate wells were added 50 µL of human plasminogen (Roche Diagnostics), 30 µL of
188 D-VLK-AMC, and 10 µL of the tested thrombolytic to initiate the reaction. The resulting
189 concentrations in microplate wells were 3.0 µM fibrin (where applicable), 0.04 UN/mL thrombin
190 (where applicable), 3.0 µM fibrinogen (where applicable), 4.5 µM plasminogen, 200 µM D-VLK-
191 AMC, and 0.08 nM tested thrombolytic. The microplate containing all the tested conditions was
192 then sealed with a transparent adhesive foil and the enzymatic activity was measured by
193 monitoring the increase in fluorescence with time using the microplate reader FLUOstar OPTIMA
194 (BMG Labtech). The emission was detected every 60 seconds at 460 nm upon excitation at 360
195 nm with the instrument gain set to 1,100 and the bottom reading position.

196 **Activity and stimulation kinetic data analysis**

197 All the curves of increasing AMC fluorescence with time were first recalculated to AMC
198 concentration changes with time based on the calibration curve that was obtained by measuring
199 fluorescence of various increasing concentrations of the AMC standard (Sigma-Aldrich) ranging

200 from 0 to 1000 μM. The concentration dependence exhibited an exponential trend, so the
201 calibration curve was constructed by fitting the calibration points with the exponential **Equation**
202 **1** to obtain the calibration factors F_a, F_b, and F_c.

$$\text{Fluorescence} = F_a \cdot (1 - e^{-F_b \cdot [\text{AMC}]}) + F_c \quad (1)$$

203 Due to the coupled nature of the applied assay, the initial phase of each recalculated kinetic
204 curve was fitted with the quadratic **Equation 2**, where v_0 corresponds to the determined initial
205 rate of the enzymatic reaction, t_0 to the dead-time between the manual mixing of the assay
206 components and the start of the measurement, and c to the initial y-axis offset. Final values of
207 initial rates (activities) were expressed as average ± standard deviation for each measured
208 sample and condition.

$$[\text{AMC}] = v_0 \cdot (t + t_0)^2 + c \quad (2)$$

209 Stimulation factors and selectivities were determined according to the previously postulated
210 definitions[24]. Stimulation factor for the fibrinogen stimulation ($Stim_{FG}$) or the fibrin stimulation
211 ($Stim_{FN}$) was calculated as a ratio of the activity in the presence of the stimulant ($v_{0,FG}$ or $v_{0,FN}$)
212 over the activity in the absence of the stimulant (v_0), as summarized in **Equation 3 and 4**.
213 Selectivity (Sel_{FN}) towards fibrin (with respect to fibrinogen) was then calculated as a ratio of
214 stimulation factors or initial rates in the presence of fibrin over fibrinogen according to **Equation**
215 **5**. The resulting value was relativized to alteplase and statistically compared using two-sample
216 *t*-test.

$$Stim_{FG} = \frac{v_{0,FG}}{v_0} \quad (3)$$

$$Stim_{FN} = \frac{v_{0,FN}}{v_0} \quad (4)$$

$$Sel_{FN} = \frac{Stim_{FN}}{Stim_{FG}} = \frac{v_{0,FN}}{v_{0,FG}} \quad (5)$$

217 **Plasminogen activator inhibitor 1 (PAI-1) inhibition resistance**

218 The potency of thrombolytic inhibition was analyzed by determining the fraction of active
219 thrombolytics at different PAI-1 concentrations. The experiment was performed at 37 °C in
220 phosphate-buffered saline PBS pH 7.4 (10 mM Na_2HPO_4, 1.8 mM KH_2PO_4, 2.7 mM KCl, 137 mM
221 NaCl) containing 1 mM $CaCl_2$, 0.0035 % L-arginine, and 0.01 % Tween 80, and each measurement
222 was repeated in three replicates. 40 µL of PAI-1 (Sigma-Aldrich) was mixed with 10 µL of a tested
223 thrombolytic and the sealed mixture was incubated at 37 °C for 60 min while shaking at 180 rpm
224 to ensure that the interaction with PAI-1 reached equilibrium. The resulting concentrations in
225 the inhibition mixture were 0–1.5 µM PAI-1 and 0.16 µM thrombolytic. Residual activity was
226 determined by transferring 10 µL of the inhibition mixture into a microplate well of a black clear
227 bottomed 96-well plate and mixing it with 40 µL of the tPA fluorogenic substrate Boc-L-(p-F)FPR-
228 ANSN-H-C_2H_5 (US Biological) to initiate the enzymatic reaction. The resulting fluorogenic
229 substrate concentration was 200 µM. The microplate was sealed with a transparent adhesive foil
230 and the enzymatic activity was detected by monitoring the increase in fluorescence over time
231 using the microplate reader FLUOstar Omega (BMG Labtech). The emission was detected every
232 60 seconds at 460 nm upon excitation at 360 nm with the instrument gain set to 580 and the
233 bottom reading position.

234 **Inhibition resistance data analysis**

235 The initial phase of each fluorescence kinetic curve was fitted with the linear **Equation 6** where
236 the slope v_i corresponds to the initial rate of the inhibited enzymatic reaction (residual activity)
237 and F_0 to the initial fluorescence offset. Since the fluorogenic substrate was converted directly
238 by the tested thrombolytic enzymes with no reaction coupling and since the fluorescence of the
239 generated product was directly proportional to its concentration, fluorescence curves could be
240 fitted directly with the linear equation to reliably obtain relative values of initial rates without
241 a need for recalculation to concentration changes. Final values of initial rates were expressed as
242 average ± standard deviation for each measured sample and condition.

$$\text{Fluorescence} = v_i \cdot t + F_0 \quad (6)$$

243 Concentration dependence of determined residual activities v_i with increasing PAI-1
244 concentration was fit with **Equation 7** for a tightly bound inhibitor where c_I corresponds to the
245 total concentration of PAI-1, c_E to the total concentration of a thrombolytic enzyme, v_i to the
246 residual activity at a given concentration c_I of PAI-1, v_0 to the non-inhibited activity in the
247 absence of PAI-1, and IC_{50} to the concentration of PAI-1 causing 50 % inhibition of a tested
248 thrombolytic. The values of IC_{50} were determined for each tested thrombolytic, relativized to
249 the value for alteplase, and statistically compared using a two-sample *t*-test.

$$c_I = c_E \cdot \left(1 - \frac{v_i}{v_0}\right) + \left(IC_{50} - \frac{c_E}{2}\right) \cdot \left(\frac{v_0}{v_i} - 1\right) \quad (7)$$

250 **Fibrin binding and affinity**

251 Affinities of thrombolytics towards fibrin were analyzed by indirectly determining the level of
252 fibrin-bound thrombolytics at various fibrin concentrations. The experiment was performed at
253 37 °C in phosphate-buffed saline PBS pH 7.4 (10 mM Na_2HPO_4, 1.8 mM KH_2PO_4, 2.7 mM KCl, 137
254 mM NaCl) containing 1 mM $CaCl_2$, 0.0035 % L-arginine, and 0.01 % Tween 80 and each
255 measurement was repeated in three replicates. 320 µL of plasminogen-free human fibrinogen
256 (HYPHEN BioMed) was premixed with 40 µL of a tested thrombolytic and the clotting was initiated
257 by the addition of 40 µL of human thrombin (Sigma-Aldrich). The resulting concentrations in the
258 polymerization mixture were 0–38 µM fibrinogen, 16 nM (alteplase, Alt01, Alt02, Alt03, AltAnc02,
259 AltEM03, DesEM01) or 235 nM (tenecteplase, Brnoteplase, DesEM02, desmoteplase) thrombolytic,
260 and 2 UN/mL thrombin. This mixture was incubated at 37 °C for 60 min while shaking at 180 rpm
261 to ensure that a complete clot formation was achieved. The clots with bound thrombolytics were
262 separated by centrifugation at 4 °C and 15,000 rpm for 30 minutes and the amount of unbound
263 thrombolytic in the supernatant was determined by residual activity measurement. 20 µL of the
264 supernatant was carefully transferred into a microplate well of a black clear bottom 96-well
265 plate and mixed with 50 µL of human plasminogen (Roche Diagnostics) and 30 µL of the
266 fluorogenic substrate D-VLK-AMC (AAT Bioquest) to initiate the enzymatic reaction. The resulting
267 concentrations in a microplate well were 2.3 µM plasminogen and 200 µM D-VLK-AMC. The
268 microplate was sealed with a transparent adhesive foil and the enzymatic activity was detected

269 by monitoring an increase of fluorescence with time using the microplate reader FLUOstar
270 OPTIMA (BMG Labtech). The emission was detected every 60 seconds at 460 nm upon excitation
271 at 360 nm with the instrument gain set to 1,100 and the bottom reading position.

272 **Fibrin binding equilibrium data analysis**

273 The values of residual plasminogen activation initial rates (activities) $v_{0,res}$, corresponding to the
274 relative amount of an unbound thrombolytic agent, were determined by fitting the kinetic curves
275 as described above in the corresponding 'Activity and stimulation kinetic data analysis' section.
276 These values were then relativized to the initial rate in the absence of fibrin ($v_{0,abs}$) according to
277 **Equation 8** in order to obtain a fraction of bound plasminogen activator (*Bind*) at a given
278 concentration of fibrin. Concentration dependence of the determined bound fraction *Bind* with
279 increasing fibrin concentration was fit with the hyperbolic **Equation 9** to obtain the value of
280 dissociation constant K_d and the percentage of the maximal fibrin binding $Bind_{lim}$. The values
281 were determined for each tested thrombolytic, relativized to the value for alteplase, and
282 statistically compared using a two-sample *t*-test.

$$\text{Bind} = \frac{v_{0,abs} - v_{0,res}}{v_{0,abs}} \cdot 100\ \% \tag{8}$$

$$\text{Bind} = \frac{Bind_{lim} \cdot [\text{fibrin}]}{K_d + [\text{fibrin}]} \tag{9}$$

283 **Preparation of clots and fibrin gel for *in vitro* assays**

284 Semi-synthetic clots were prepared by mixing human fibrinogen (Tisseel Lyo kit, Baxter, dissolved
285 in water for injection to reach the concentration of 52 mg/mL), human thrombin (Tisseel Lyo
286 kit, Baxter, dissolved in 40 μM $CaCl_2$ solution to the concentration of 3.3 IU/mL), and red blood
287 cells (RBCs) isolated from healthy donors' blood in the volume ratio of 1:1:1. The incubation and
288 clotting were performed in plastic Eppendorf tubes (0.5 mL for static model; 0.2 mL for flow
289 model) for 30 min at 37 °C and >90 % relative humidity under static conditions. The prepared
290 clots were immediately introduced into the model. The final concentrations of components in

291 the prepared clots were 17.3 mg/mL fibrinogen, 1.1 IU/mL thrombin, and $4.2 \cdot 10^9$ RBCs/mL and
292 the total clot volume was 90 µL for the static model and 60 µL for the flow model.

293 RBC dominant clots were prepared from 200 µL of healthy donors' whole blood without
294 anticoagulant by clotting in borax glass tubes (inner diameter 8 mm) for 3.5 h at 37 °C and >90
295 % relative humidity under static conditions. The prepared clots were immediately introduced
296 into the model.

297 Fibrin gel was prepared from the mixture of fibrinogen (Tisseel Lyo kit, Baxter, dissolved in water
298 for injection to the concentration of 34.6 mg/mL) and thrombin (Tisseel Lyo kit, Baxter, dissolved
299 in 40 µM $CaCl_2$ solution to the concentration of 2.2 IU/mL) in the volume ratio of 1:1. The
300 incubation and the clotting was performed inside micro-slide channels for 30 min at 37 °C and
301 >90 % relative humidity under static conditions. The final concentrations of the components in
302 the prepared fibrin gel were 17.3 mg/mL fibrinogen and 1.1 IU/mL thrombin and the total volume
303 per micro-slide channel was 30 µL.

304 All blood donors had agreed to donate blood samples on the premise of signed informed consent
305 for the collection of blood. Individuals, who had received acetylsalicylic acid, non-steroidal anti-
306 inflammatory, or antiplatelet drugs within 7 days before blood collection, were excluded.

307 ***In vitro* thrombolytic models**

308 Thrombolytic experiments were performed in static and flow *in vitro* models that were described
309 in contemporary literature[25,26] but were optimized to determine the suitably measurable effect
310 of alteplase in a highly reproducible manner, as reported in previous publications[27-30]. Briefly,
311 the static model consisted of 1.5 mL plastic Eppendorf tubes filled with fresh frozen human
312 plasma (177RM, Monobind Inc.) medium to a total volume of 500 µL, in which the clots were
313 individually incubated. The tubes were incubated at 37 °C in a dry-block incubator for 60 minutes
314 (the same amount of time as indicated for alteplase treatment of stroke patients).

315 The flow model consisted of silicone chips made of Sylgard 184 Silicone Elastomer (Dow Corning),
316 which were prepared according to human middle cerebral artery anatomy, with narrowings
317 dimensionally based on patient CT scans (n = 4). The bifurcation was included to enable

318 permanent circulation in the system. Each silicone chip was connected by plastic pipes (internal
319 diameter 3.1 mm) to the 8-channel pump head peristaltic pump MINIPULS 3 (Gilson Inc.), and
320 the entire system was maintained at 37 °C for incubation lasting 180 min. This arrangement
321 maintained the hydrodynamic forces involved in clot removal[31], whereby a pressure gradient of
322 10 mm Hg was generated across the occlusion.

323 Both semi-synthetic and red blood cell dominant clots (preparation described in the
324 corresponding 'Preparation of clots and fibrin gel for in vitro assays' section above) were
325 separately employed in both thrombolytic models and the thrombolytic efficiencies were
326 compared. The final concentrations of tested thrombolytic enzymes were selected to be
327 consistent with the clinically relevant dosage indicated for patients with ischemic stroke (1.3
328 µg/mL), according to the manufacturer's instructions and supporting pharmacokinetic data[32].
329 Alternatively, 10-fold lower and 2-, 5-, 10-, and 50-fold higher concentrations were tested as
330 well.

331 ***In vitro* lytic efficacy analysis**

332 Clot lysis in the static model was determined by measuring clot mass loss[26–28,30,33] and by
333 spectrophotometric determination of RBC release into the incubation medium at 575 nm[27,28,30].
334 Clot lysis in the flow model was determined by measuring recanalization time, clot length
335 changes, and spectrophotometric determination of RBC release[27,29,30]. Recanalization frequency
336 was determined as a percentage ratio of complete recanalization to the total number of samples
337 in the respective treatment group. Relative clot reduction was determined as a percentage of
338 clot area reduction prior to clot release from the narrowed occlusion site. In addition, the
339 thrombolysis rate was calculated using linear regression of relative clot reduction at 10-minute
340 intervals. Data were expressed as mean ± standard deviation, if not otherwise indicated. The
341 generated box plots were presented as mean value (cross), median (line), interquartile range
342 (box), and minimum and maximum value (whiskers). ANOVA with post-hoc Tukey's HSD test was
343 used to compare data. P-values ≤ 0.05 were considered to be statistically significant. All analyses
344 were performed using GraphPad Prism (GraphPad Software Inc.).

345 ***In vitro* penetration microarray**

346 Penetration experiments were performed in the microarray model outlined in recent literature[34-]
347 [38] and optimized to provide a suitably measurable effect of alteplase in a highly repeatable
348 manner. The microarray consisted of the microslide µ-Slide VI 0.4 (ibidi GmbH) containing
349 channels that were filled with a prepared fibrin gel (procedure described in the corresponding
350 'Preparation of clots and fibrin gel for in vitro assays' section above). Fluorescently labelled
351 plasminogen activators or bovine serum albumin (A9418, Sigma-Aldrich), as a relevant fibrin non-
352 interacting control, were applied to individual microslide channels and fluorescence intensities
353 were continuously recorded in 5 min intervals for 180 min, at 0.25 mm distance intervals up to
354 1.00 mm from the application site. The fluorescence signal was recorded using the microscope
355 ZEISS Axio Observer Z1 (Carl Zeiss AG) equipped with the metal halide fluorescence light source
356 HXP 120 (Carl Zeiss AG) and the high efficiency Filter Set 43 HE (Carl Zeiss AG). The detection
357 settings were as follows: excitation BP 550/25; beam splitter FT 570; emission BP 605/70.
358 Thrombolytic proteins and bovine serum albumin control were fluorescently labelled with
359 rhodamine B isothiocyanate (283924, Sigma-Aldrich) prior to the penetration assay according to
360 the standard labeling protocol provided by the manufacturer. The final concentrations of the
361 labelled proteins were the same as for thrombolytic experiments, i.e., 1.3 µg/mL. Thrombolytic
362 efficiencies of labelled plasminogen activators were verified in the static model.

363 **Penetration rate analysis**

364 Plasminogen activator penetration rate through the fibrin gel was determined by continuous
365 measurements of fluorescence intensities at a distance of up to 1 mm from the front of the
366 plasminogen activator application site[30]. The penetration rate was expressed as the relative
367 fluorescence intensity (RFI) at a given distance and time. RFI was determined using a custom
368 image analysis script in the Python programming language. Penetration rate data were further
369 normalized to relevant controls. Data were expressed as mean ± standard deviation, if not
370 otherwise indicated. The generated box plots were presented as mean value (cross), median
371 (line), interquartile range (box), and minimum and maximum value (whiskers). ANOVA with post-
372 hoc Tukey's HSD test was used to compare data. P-values ≤ 0.05 were considered to be

373 statistically significant. All analyses were performed using GraphPad Prism (GraphPad Software
374 Inc.).

375 **Preparation of clots for *in vivo* assays**

376 Details of the characteristics and nature of artificial clots are the subject of a previous project[39],
377 and their preparation is therefore described only briefly. Commercial human fibrin glue Tisseel
378 kit (Baxter) was used to generate artificial clots for *in vivo* experiments. Saline solution (1.5 mL)
379 and $BaSO_4$ suspension (0.5 mL) (Micropaque, Guerbet) were injected into the original "TISSEEL"
380 ampoule. 1 mL of the original calcium chloride solution and 5 mL of bovine serum were injected
381 into the "Thrombin 500 I.U." original ampoule. Finally, "TISSEEL" and "Thrombin 500 I.U."
382 preparations were injected in a 1:1 ratio into a PE60 and PE10 tubes (Braintree Scientific) for
383 the thrombolytic effectivity study and the safety study, respectively, using the original Duploject
384 system (Baxter). Both ends of the cannula containing clot components were hermetically sealed
385 to prevent any evaporation or desiccation, and the mixture was incubated at 37 °C for 120 min,
386 followed by storage at 4–8 °C for additional 24 hours. The resulting artificial clot was cut into
387 10 mm fragments for the effectivity study and 1 mm fragments for the safety study and the
388 corresponding samples were stored in the saline solution in an Eppendorf tube at –20 °C.

389 **Thrombolytic effectivity study *in vivo***

390 Adult male outbreed Wistar rats (n=68; body weight 120–180 g) were selected for the *in vivo* lysis
391 experiments and were randomized into groups with different treatment regimens (variable
392 thrombolytic types, doses, and administration routes) as described in **Table 1**.

393 **Table 1: Overview of animal experimental groups for in vivo effectivity study based on different treatment**
394 **regimes.** CRI = continuous rate infusion.

Experimental group	Number of animals in the group
Control group (saline solution)	10
Alteplase (0.9 mg/kg, CRI)	16
Tenecteplase (0.25 mg/kg, bolus)	12
Brnoteplase (0.9 mg/kg, CRI)	4
Brnoteplase (0.9 mg/kg, bolus)	12
Brnoteplase (2.5 mg/kg, bolus)	12
Brnoteplase (5.0 mg/kg, bolus)	2

395 The exclusion criterion for the experiment was death during the anesthesia or the surgical
396 procedures before the clot delivery. Throughout the thrombolysis experiment, rats were under
397 general anesthesia induced by inhalation of 2.5 % isoflurane in filtered room air as a carrier gas.
398 After the intramuscular application of xylazine and ketamine (5 mg/kg and 35 mg/kg of body
399 weight, respectively), a mixture of urethane (80 mg/mL) and alpha-chloralose (6 mg/mL) at a
400 dose of 8 mL/kg of body weight was applied into the peritoneal cavity. Subsequently, the left
401 common carotid artery (CCA) was dissected, visualized, and cannulated in a retrograde direction
402 with a PE50 (Braintree Scientific) cannula.

403 Three individual barium-labeled artificial clots were injected via the PE50 catheter cannula into
404 the aortic arch of each tested rat. Micro-fluoroscopy using the C-arm LabScope system
405 (Glenbrook Technology, Inc.) was used to verify the localization of the introduced clots in the
406 branches of the abdominal aorta and the position of the animals was then adjusted to achieve
407 the optimal visibility of the clots with the maximum area of their size and without the shielding
408 of bone structures. The initial image was captured at time zero (before the thrombolytic drug
409 administration). Subsequently, a bolus injection/continuous rate infusion of a tested
410 thrombolytic was initiated. The continuous rate infusion treatment consisted of an initial bolus
411 of 10 % of the total dose volume, followed by an infusion of the remaining 90 % volume for 60
412 minutes. In the bolus treatment groups, the entire volume of the thrombolytic agent was
413 administered at once. The control group received an equivalent volume of intravenous saline
414 solution. The therapy was monitored for 60 minutes by the C-arm micro-fluoroscopy and
415 radiographs were acquired and stored every 5 minutes.

416 ***In vivo* thrombolytic effectivity study outcome analysis**

417 The outcome was measured as a relative area change of each monitored artificial clot, and the
418 lysis rate was then calculated as a linear fit of relative area change over time. All collected
419 radiographs were analyzed using the ImageJ 1.52a software (Wayne Rasband, National Institutes
420 of Health), and the area of identified clots in pixels was manually determined at each time point.
421 All images of one animal were measured simultaneously in one reading sequence. Two
422 independent observers performed the image analysis, blinded to one another's results and to

423 animal group assignment. Anatomical determination of arteries with clots was performed after
424 all measurements. A standardized protocol was established and followed for non-standard clot
425 positions or movements: (1) If the area of two clots in different arteries overlapped, the size was
426 measured as a single clot. (2) If the clot changed position due to animal/intestinal movement or
427 projection angle, the area of the clot was recalculated to the adjusted change of the nearest
428 bone shadow. The image was excluded if no bone was present. (3) If the lysis of the clot caused
429 its movement but the clot was still visible on the image, the shadow area of the clot was included
430 in the original area of the clot. The image was excluded if the clot moved out of the image.

431 The change in the artificial clot area (CAC) was calculated from the clot area at a calculated
432 time (a_t) relative to the clot area at time zero baseline before thrombolytics administration (a_0),
433 i.e., at the beginning of the experiment, based on **Equation 10**. The lysis rate in $\%.min^{-1}$
434 represents a relative change in the area of the artificial clot (CAC) divided by the minute in which
435 the area was measured (t) based on **Equation 11**. Results of the thrombolysis were used to
436 generate the thrombolytic curve. The area under the thrombolytic curve (AUC) was calculated
437 and used as a comparative parameter among the tested and control groups. All analyses were
438 performed using Excel for Microsoft 365 MSO version 2405 (Microsoft Corporation) and GraphPad
439 Prism version 8.0.0 (GraphPad Software Inc.).

$$CAC = \frac{a_0 - a_t}{a_0} \cdot 100\ \% \tag{10}$$

$$\text{lysis rate} = \frac{CAC}{t} \tag{11}$$

440 **Safety study**

441 The safety study was based on a thromboembolic Middle Cerebral Artery Occlusion (MCAO)
442 model, utilizing the same clot type as in the thrombolytic effectivity study. However,
443 embolization to all major cerebral arteries, namely the anterior, middle, and posterior cerebral
444 arteries, was included. This approach is referred to as the **C**ircle **o**f **W**illis **B**ranches **O**cclusi**o**n -
445 CoWBOi model. Male outbred Wistar rats, weighing between 480 and 980 grams and aged 7 to 9
446 months, were housed individually under standard conditions, with a natural light/dark cycle and

447 unrestricted access to food and water. Animals were randomly assigned to one of three
448 experimental groups, receiving either alteplase (0.9 mg/kg, continuous rate infusion, n=25,
449 included n=22), tenecteplase (0.25 mg/kg, bolus, n=25, included n=24), or Brnoteplase (2.5
450 mg/kg, bolus, n=23, included n=22). Rats, that did not develop cerebral stroke or died within
451 120 minutes of thrombolytic treatment, were excluded from the study.

452 General anesthesia was induced via inhalation of 2.5 % isoflurane, followed by intramuscular
453 administration of xylazine (5 mg/kg), ketamine (35 mg/kg), and intraperitoneal diazepam (2
454 mg/kg). Embolization was performed in a modified version of the standard MCAO model, with
455 cannulation of the left external, and internal carotid arteries. Two embolic clots (1.5 mm × 0.3
456 mm) were introduced into the intracranial internal carotid artery. Thrombolytic treatment was
457 initiated 4 hours post-embolization. After 24 hours, the animals were euthanized, and their
458 brains were collected in cold saline without flushing. As described previously, the extracted
459 brains were fixed in formalin for 24 hours and stained with iodine[40] . In contrast with the original
460 set-up, the brains were not examined in agarose but in paraffin oil. Micro-computed tomography
461 (miCT) imaging was performed using a SkyScan1276 CMOS (Bruker) scanner, and the acquired
462 scans were analyzed using the Amira software (Thermo Scientific). Examiners were blinded to
463 group assignments to ensure unbiased assessment.

464 ***In vivo* safety study outcome analysis**

465 To evaluate hemorrhagic transformation (HT), a classification system based on ECASS II criteria[11]
466 was applied. Hemorrhagic transformation was categorized into four subtypes (HI1, HI2, PH1, and
467 PH2) according to the criteria listed in **Table 2**. Considering that thrombolytic enzymes were
468 administered 4 hours after clot embolization, by which time all collateral vessels had already
469 closed due to ischemic damage, successful recanalization in this model was consistently
470 associated with hemorrhagic transformation.

471

472

473 **Table 2: Hemorrhagic transformation (HT) classification based on the ECAS II study**. The classification
474 recognizes four HT subtypes (HI1, HI2, PH1, and PH2) that differ in the listed criteria.

Grade	Description
HI1	Petechial hemorrhages at infarct margins
HI2	Petechial hemorrhages throughout the infarct without mass effect
PH1	Hemorrhage affecting ≤30 % of the infarcted area with minor mass effect
PH2	Hemorrhage affecting >30 % of the infarcted area with substantial mass effect

475

476 To quantify hemispheric asymmetry (HA), we calculated the affected hemisphere volume
477 (*affected*) and the intact hemisphere volume (*intact*), excluding the olfactory bulbs and
478 cerebellum from the analysis. The percentage of HA was then derived using **Equation 12**. A
479 hemispheric asymmetry of 6 % was identified as the threshold distinguishing normal from
480 pathological brains. Values exceeding this threshold were consistently associated with the
481 presence of cerebral edema.

$$\mathrm{HA} = \frac{\text{affected - intact}}{\text{intact}} \cdot 100\ \% \tag{12}$$

482 **Quantification of residual plasminogen, plasmin, and thrombolytic levels in rat plasma**

483 At the end of the *in vivo* thrombolytic effectivity study, whole blood from the common carotid
484 was collected to a K3-EDTA tube (2.7 mL, S-Monovette, Sarstedt AG). The collected blood was
485 centrifuged for 15 min at 1,500 rpm and the resulting plasma was separated into an Eppendorf
486 tube, aliquoted, and stored at -20 °C. The collected plasma samples were tested for levels of
487 plasmin, plasminogen, and a thrombolytic enzyme using ELISA Rat Plasmin Kit (MyBioSource),
488 ELISA Rat Plasminogen Kit (MyBioSource), and ELISA Human Active tPA Kit (Molecular
489 Innovations), respectively. The determination of the concentration was performed according to
490 the protocol provided by the manufacturer with no modifications. In the case of Human tPA Kit,
491 purified solutions of alteplase and Brnoteplase (the same as administered in rats) with known
492 concentrations were used to generate individual calibration curves to prevent any discrepancies
493 caused by different sources of the administered and the calibration samples. The final plasma
494 levels were calculated from the measured absorbance values based on the constructed
495 calibration curves.

496 **Consent for animals used in experiments**

497 All procedures and animal experiments were performed in full compliance with the ARRIVE and
498 the European Community Council Directive (2010/63/EU) for Protection of Vertebrate Animals
499 Used for Experimental and other Scientific Purposes guidelines. The project was approved by the
500 Masaryk University Brno Institutional Committee for the Protection of Experimental Animals and
501 by the Committee for the Protection of Experimental Animals of the Ministry of Education Youth
502 and Sports in the Czech Republic (MEYS CZ) with the protocol number MSMT-35804 / 2019-2.

503 # Results

504 **Computational design selects the most promising thrombolytic candidates**

505 The initial pool of novel thrombolytic variants for experimental testing was designed and selected
506 *in silico* using three independent computational strategies: (i) rational design, (ii) ancestral
507 sequence reconstruction, and (iii) database mining (**Table 3**, **Figure S1**).

508 **Rational design** focused on reducing interactions with clearance and signaling receptors,
509 particularly LRP1 and NMDAR, which are implicated in short half-life and neurotoxicity. This was
510 achieved by introducing Tyr67Asn and Ser69Ala mutations shown to prevent glycosylation
511 responsible for LRP1 binding[41] (resulting in variant Alt03), and by combining these mutations with
512 additional substitutions of lysine residues (variants Alt01 and Alt02). Lysine residues are known
513 to mediate LRP1 interaction. Alt01 includes additional Lys10Glu, Lys49Ile, and Lys152Gln
514 mutations which were selected using structure-based computational tools, namely protein-
515 protein docking, molecular dynamics, surface exposure analysis, and thermodynamic stability
516 predictions (**Supplementary Note 1**). Alt02 incorporates additional Lys82Ala, Lys159Ser, and
517 Lys162Ile mutations selected based on their sequence conservation in desmoteplase, which has
518 been shown to compete with alteplase for the LRP1 binding site[42] (**Supplementary Note 2**).
519 Finally, the Brnoteplase variant was constructed by combining the two original substitutions
520 preventing LRP1-binding glycosylation[41] (Tyr67Asn and Ser69Ala) with mutations decreasing PAI-
521 1 inhibition and increasing fibrin specificity[45] (Lys296Ala, His297Ala, Arg298Ala, Arg299Ala),

522 disabling NMDAR-mediated neurotoxicity[44] (Trp253Arg), and removing high-mannose
523 glycosylation responsible for the low alteplase biological half-life[43] (Asn117Gln).

524 **Ancestral sequence reconstruction (ASR)** strategy utilized the FireProt[ASR] webserver to
525 explore evolutionary and functional diversity while preserving thrombolytic activity. The analysis
526 produced a phylogenetic tree comprising 150 extant alteplase homologs and 149 ancestral
527 sequences (**Figure S2**). Two ancestral nodes close to alteplase, named AltAnc01 and AltAnc02,
528 were selected based on sequence identity and conservation of catalytic residues (**Table 3**).
529 AltAnc01 is ancestral to alteplase and four other extant sequences annotated as plasminogen
530 activators (PAs), while AltAnc02 is ancestral to alteplase, ten additional annotated PAs, and one
531 hypothetical protein predicted to be a PA (**Supplementary Note 3**).

532 **Table 3: Summary of *in silico* designed and selected thrombolytics for experimental testing.** Variants
533 highlighted in grey could not be experimentally produced and therefore were not further characterized. Full
534 sequences of all variants are provided in **Figure S1**. ASR = ancestral sequence reconstruction.

Variant naming	Modification strategy	Parental Protein	Sequence modification
Alt01	Rational design	Alteplase	K10E/K49I/Y67N/S69A/K152Q
Alt02	Rational design	Alteplase	Y67N/S69A/K82A/K159S/K162I
Alt03	Rational design	Alteplase	Y67N/S69A
Brnoteplase	Rational design	Alteplase	Y67N/S69A/N117Q/W253R/K296A/H297A/R298A/R299A
AltAnc01	ASR	Alteplase	76.6 % identity to alteplase; ancestral to 5 extant genes
AltAnc02	ASR	Alteplase	71.0 % identity to alteplase; ancestral to 12 extant genes
AltEM01	Database mining	Alteplase	78.4 % identity to alteplase; gene isoform X1 from bottlenose dolphin
AltEM02	Database mining	Alteplase	82.7 % identity to alteplase; gene isoform X2 from bottlenose dolphin
AltEM03	Database mining	Alteplase	92.0 % identity to alteplase; gene from Bolivian squirrel monkey
DesEM01	Database mining	Desmoteplase	68.0 % identity to alteplase; gene isoform X3 from Angolan colobus monkey
DesEM02	Database mining	Desmoteplase	80.0 % identity to alteplase; gene from white-winged vampire bat

535 **Database mining** using the EnzymeMiner webserver identified naturally occurring homologs
536 of alteplase and desmoteplase with potentially favorable biochemical features. Over 10,000
537 mined sequences were filtered based on predicted solubility, absence of transmembrane regions,

538 and preservation of essential catalytic domains and residues, resulting in 198 alteplase and 615
539 desmoteplase homologs meeting these criteria. From these, we manually selected five
540 candidates (**Table 3**): three homologous to alteplase (AltEM01–03) and two to desmoteplase
541 (DesEM01–02). The selected sequences originate from bottlenose dolphin, Bolivian squirrel
542 monkey, Angolan colobus, and vampire bat (**Supplementary Note 4**).

543 **Biochemical characterization identifies an improved alteplase variant Brnoteplase**

544 Gene sequences encoding putative and mutant plasminogen activators selected *in silico* were
545 experimentally constructed, and 8 out of 11 selected thrombolytic proteins were successfully
546 produced recombinantly. Our comprehensive biochemical characterization (**Figure 2**, **Table S1**)
547 revealed that all the proteins exhibited clear thrombolytic activity (**Figure 2a**, **Figure S3**, **Table**
548 **S1**), validating the robustness of our computational approach for accurately predicting and
549 designing plasminogen activator enzymes. Thermal stabilities of all characterized proteins
550 (**Figure 2d**, **Figure S4**, **Table S1**) were highly above the physiological temperature, allowing their
551 administration to the human body without a risk of rapid thermal inactivation.

552 Fibrinogen and fibrin stimulation analysis (**Figure 2b**, **Figure S3**, **Table S1**) yielded
553 unimpaired profiles for Alt01–03 compared to alteplase ($p=0.37$, $p=0.35$, $p=0.49$, respectively),
554 whereas other variants showed significantly lower fibrin stimulation ($p<0.001$) and activity
555 ($p<0.001$), suggesting inefficient thrombolysis on fibrin clots. Remarkably, the variant
556 Brnoteplase displayed minimal activity with no stimulation and when stimulated by fibrinogen,
557 but it was massively stimulated by fibrin, 5.2-fold more than alteplase ($p<0.001$). This resulted
558 in an extraordinary fibrin selectivity of Brnoteplase (**Figure 2c**, **Figure S3**, **Table S1**) that was
559 similar to highly selective thrombolytics desmoteplase and tenecteplase.

560 All four sufficiently fibrin-active variants, Alt01–03 and Brnoteplase, further exhibited
561 significantly increased resistance to PAI-1 inhibition ($p<0.001$) and reduced fibrin binding
562 ($p<0.001$) compared to alteplase, indicating improved potential for clot penetration and lysis
563 throughout the entire volume from inside. The highest inhibition resistance was observed for the
564 variant Brnoteplase (**Figure 2e**, **Figures S5 and S6**, **Table S1**), while the most pronounced

565 reduction in fibrin binding was observed for Alt01, followed by Brnoteplase (**Figure 2f**, **Figures**
566 **S7 and S8**, **Table S1**).

567 In summary, the set of biochemical assays identified an exceptional alteplase variant,
568 Brnoteplase, with several favorable clinical implications over alteplase: (i) 80-fold enhanced
569 fibrin selectivity, (ii) 4-fold increased resistance to PAI-1 inhibition, and (iii) 4-fold improved
570 penetration potential.

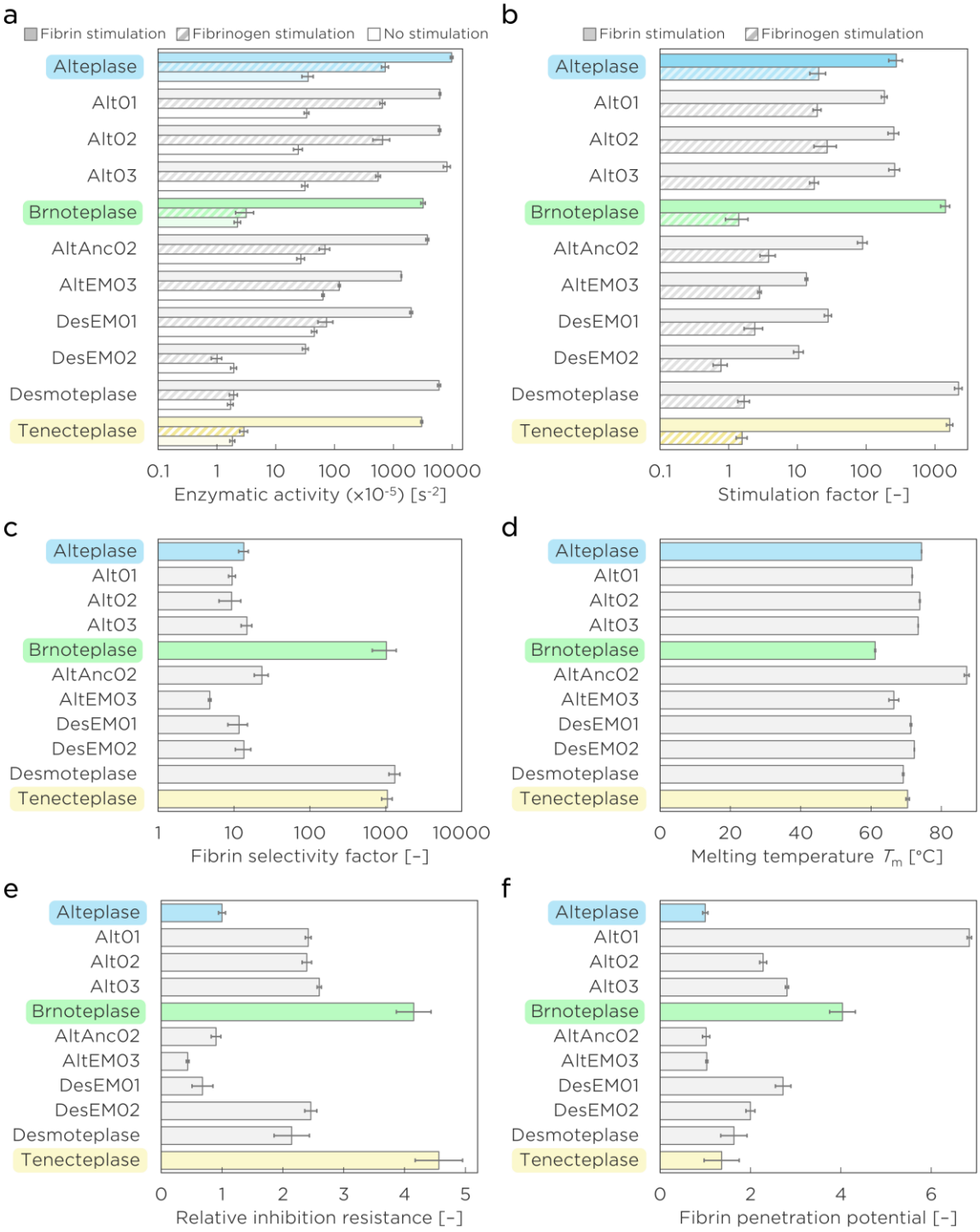

Figure 2: Biochemical characterization of thrombolytic variants. (**a**) Comparison of plasminogen activation enzymatic activities (dark solid bars) and their values in the presence of fibrinogen (hatched bars) and fibrin (light solid bars) stimulants. (**b**) Comparison of fibrinogen (solid bars) and fibrin (hatched bars) stimulation factors. The factors are defined as fibrin(ogen)-stimulated activity over non-stimulated activity ratios. (**c**) Comparison of fibrin selectivity factors. (**d**) Comparison of melting temperatures T_m values, defining protein thermal stabilities. At T_m, half of the protein molecules are unfolded. (**e**) Relative comparison of inhibition resistance towards plasminogen activator inhibitor-1 (PAI-1) calculated as a ratio of the IC_{50} value for a tested protein over the IC_{50} value for alteplase (reference benchmark protein). (**f**) Relative comparison of fibrin penetration potential calculated as a ratio of the fibrin dissociation constant (K_d) value for a tested protein over the fibrin K_d value for alteplase (reference benchmark protein). Clinically used variants alteplase and tenecteplase are highlighted in blue and yellow, respectively. The variant Brnoteplase, which was selected for further *in vitro* and *in vivo* testing, is highlighted in green. Brnoteplase exhibited superior fibrin stimulation, fibrin selectivity, PAI-1 inhibition resistance, and penetration potential. Please note the logarithmic scale of the x-axis in (**a**), (**b**), and (**c**). The bars represent mean values and the whiskers correspond to standard errors.

586 ***In vitro* thrombolysis and penetration confirm enhanced Brnoteplase properties**

587 Alt01–03 and Brnoteplase, the four variants identified as highly fibrin-active in biochemical
588 assays, were subjected to thrombolysis testing on *in vitro* prepared human clots and compared
589 to alteplase and tenecteplase (**Figure 3**). Treatment with all the tested thrombolytics in the
590 static model containing semi-synthetic clots provided significantly greater clot mass loss
591 ($p<0.001$) and red blood cell (RBC) release ($p<0.001$) compared to the untreated group (**Figure**
592 **3a**, **Figure S9**, **Table S2**). The results of lysis efficiencies were consistent with the biochemical
593 characterization data (**Figure 2a**).

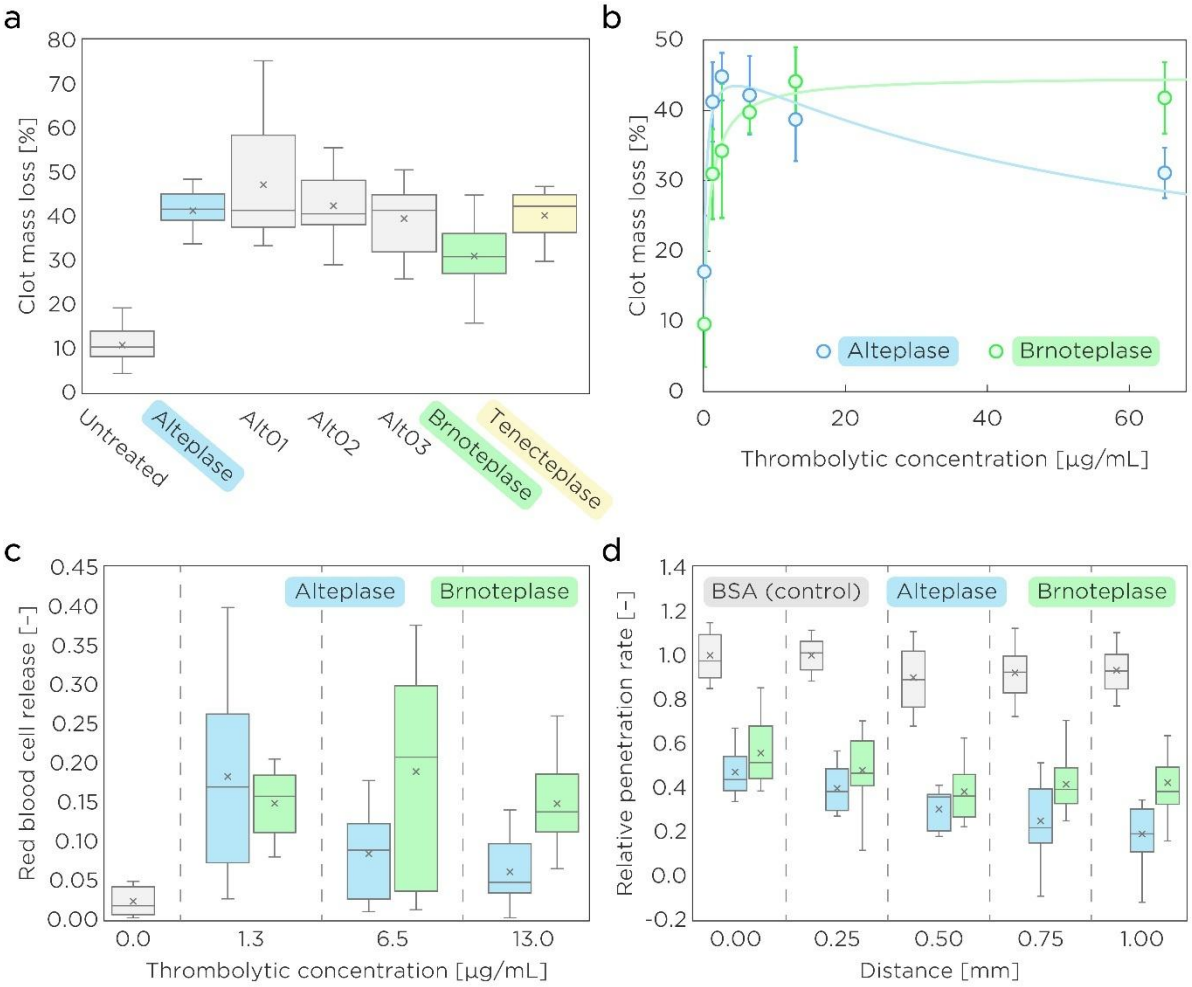

594
595 **Figure 3: *In vitro* analysis of thrombolysis efficacy and fibrin penetration.** (**a**) Comparison of thrombolytic
596 efficacy in the static model with semi-synthetic clots expressed as clot mass loss. (**b**) Concentration dependence
597 profile of thrombolytic efficacy with increasing applied concentration of a tested thrombolytic in the static
598 model. (**c**) Comparison of thrombolytic efficacy at multiple concentrations in the flow model expressed as red
599 blood cell release. (**d**) Comparison of relative penetration rates at multiple distances of a fibrin gel. Box plots
600 illustrate mean values (cross), median (line), interquartile range (box), and minimum/maximum values
601 (whiskers). Scatter plots illustrate mean values (circle) and standard errors (whiskers).

602 The concentration dependence experiment with alteplase and the most promising variant
603 Brnoteplase (**Figure 3b**, **Table S3**) revealed notable differences between the two tested
604 proteins. Alteplase showed no significant enhancement of thrombolysis with increasing
605 concentration, as clot mass loss at 2.6, 6.5, and 13 μg/mL was comparable to the clinically
606 relevant concentration of 1.3 μg/mL ($p=0.93$, $p>0.99$, $p=0.97$, respectively) and it even
607 decreased at the highest applied concentration of 65 μg/mL ($p=0.002$). In contrast, Brnoteplase
608 exhibited a clear trend of increasing thrombolytic efficacy with increasing dosing: clot mass loss
609 was comparable to the clinically relevant concentration only at 2.6 μg/mL ($p=0.96$) while
610 significantly greater lysis was observed at 6.5, 13, and 65 μg/mL ($p=0.02$, $p<0.001$, $p<0.001$,
611 respectively). At higher concentrations of 6.5 and 13 μg/mL, Brnoteplase reached the
612 comparable level of lysis as for alteplase ($p>0.99$, $p=0.20$, respectively), and it even surpassed
613 alteplase efficiency at the highest concentration of 65 μg/mL ($p=0.009$).

614 Similar trends were observed for RBC release analysis with semi-synthetic clots (**Figure S10a**,
615 **Table S3**) and RBC-dominant clots (**Figure S10bc**, **Table S4**), confirming the validity of the
616 measured data (details in **Supplementary Note 5**). In the flow model (**Figure 3c**, **Figure S11**,
617 **Table S5**), alteplase provided lower recanalization time ($p=0.005$), greater clot reduction rate
618 ($p<0.001$), and greater RBC release ($p=0.006$) compared to the untreated group only at the
619 clinically relevant concentration (1.3 μg/mL), while higher concentrations yielded no significant
620 effect compared to the untreated group. In contrast, Brnoteplase was significantly more
621 effective than the untreated group across all tested concentrations (details in **Supplementary**
622 **Note 6**), supporting the concentration-dependent trend observed in the static model (**Figure**
623 **3b**).

624 No significant changes in Brnoteplase thrombolytic efficacy were detected even after 3
625 months of storage at 4 °C ($p=0.40$), as opposed to alteplase ($p=0.02$), concluding the high shelf-
626 life of Brnoteplase and its suitability for long-term storage applications (**Figure S12**, **Table S6**).

627 Fibrin gel penetration experiments (**Figure 3d**, **Table S7**) confirmed detectable interaction
628 with fibrin for both alteplase and Brnoteplase, as both exhibited significant changes in
629 penetration rates ($p<0.001$ at all distances) compared to the non-interacting control bovine

630 serum albumin (BSA). Comparison of alteplase and Brnoteplase showed similar penetration rates
631 for both proteins up to the distance of 0.50 mm (p=0.07 at 0.00 mm; p=0.08 at 0.25 mm; p=0.06
632 at 0.50 mm). However, a significantly higher amount of Brnoteplase penetrated beyond 0.75 mm
633 (p=0.008 at 0.75 mm; p<0.001 at 1.00 mm), confirming the superior clot penetration potential
634 identified during biochemical characterization (**Figure 2f**).

635 Altogether, *in vitro* analysis confirmed the strong potential of Brnoteplase due to multiple
636 additional advantageous properties over alteplase: (i) thrombolytic efficacy increase with
637 concentration, (ii) preserved stability for over 3 months at 4 °C, and (iii) faster penetration rate
638 and greater distribution within the clot. Combined with its enhanced fibrin selectivity (**Figure**
639 **2c**) and PAI-1 inhibition resistance (**Figure 2e**), the Brnoteplase profile was indicating improved
640 safety, recanalization potential, and biological half-life, which would enable bolus
641 administration and increased dosing in the subsequent *in vivo* testing.

642 **Animal testing verifies increased Brnoteplase efficiency and safety *in vivo***

643 Our selected variant Brnoteplase and approved drugs alteplase and tenecteplase were tested *in*
644 *vivo* for thrombolysis effectivity and safety in rat models (**Figure 4**). Thrombolytic effectivity
645 was assessed by the lysis rate of administered thrombi and the area under the curve (AUC) of
646 lytic curves. The Brnoteplase group (2.5 mg/kg, bolus) showed a lysis rate of 1.3 ± 0.4 %/min
647 (**Figure 4a**, **Table S8**), which was the highest among groups when compared to 0.9 ± 0.5 %/min
648 lysis rate for the alteplase (0.9 mg/kg, continuous rate infusion) and 1.1 ± 0.5 %/min for
649 the tenecteplase (0.25 mg/kg, bolus) groups. Similarly, the AUC in Brnoteplase-treated rats was
650 2350 ± 720, significantly surpassing values observed in the alteplase (1520 ± 810)
651 and tenecteplase (2180 ± 1060) groups (**Figure 4a**, **Table S8**). Statistical analysis confirmed that
652 Brnoteplase demonstrated superior thrombolytic efficacy across all tested doses (0.9, 2.5, and
653 5.0 mg/kg; **Figure S13**, **Table S8**) by providing significantly higher lysis rates and AUC values
654 than both control and alteplase groups ($p \leq 0.01$). Interestingly, Brnoteplase (0.9 mg/kg)
655 demonstrated activity at the level of untreated control when applied in the continuous rate
656 infusion mode (**Table S8**).

The safety study assessed the overall incidence of hemorrhagic transformation (HT) and its severity according to ECASS II criteria[46] to evaluate the safety profile of each thrombolytic agent (**Figure 4b**, **Figure S14**, **Table S9**). Given the experimental model, in which the blood-brain barrier was damaged and collaterals collapsed due to prolonged ischemia, bleeding could not occur without recanalization[47], making overall HT incidence an indicator of successful recanalization. HT occurred most frequently (86 %) in the Brnoteplase group (2.5 mg/kg), followed by the 71 % incidence in the tenecteplase (0.25 mg/kg), and 64 % in the alteplase (0.9 mg/kg) groups, being positively correlated with recanalization frequencies (87 %, 68 %, and 56 %, respectively; **Figure S14**, **Table S9**). Among HT subtypes, Brnoteplase treatment led predominantly to mild petechial hemorrhages (HI1), occurring in 60 % of treated rats, while only 15 % resulted in severe hemorrhages (PH1). These results substantially differed from both alteplase (43 % HI1 vs. 21 % PH1) and tenecteplase (24 % HI1 vs. 35 % PH1) groups where the proportion of severe PH1 was more prevalent (**Figure 4b**, **Table S9**).

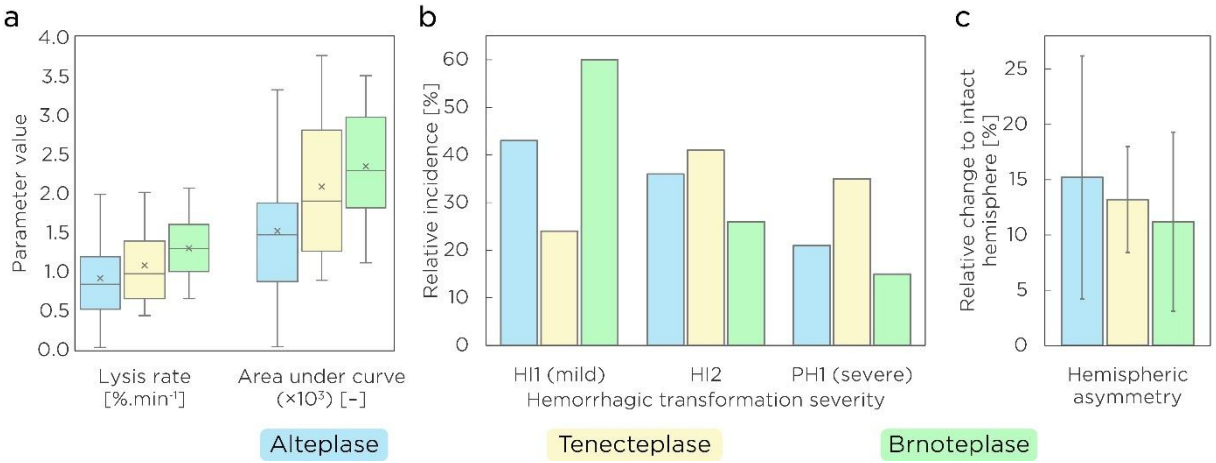

Figure 4: *In vivo* analysis of alteplase, tenecteplase, and Brnoteplase performance in animal rat models. (**a**) Comparison of the thrombolytic effectivity expressed as lysis rate (% of the clot dissolved per minute) and the area under the curve (AUC) of the lytic curve. (**b**) Proportion of hemorrhagic transformation severities according to ECASS II scoring system[46]. For a detailed description, see the Methods section. (**c**) Comparison of hemispheric asymmetry of rat brains expressed as a relative change to an intact hemisphere. Box plots illustrate mean values (cross), median (line), interquartile range (box), and minimum/maximum values (whishers). Bar plots illustrate mean values (bars) and standard errors (whiskers).

Hemispheric asymmetry analysis (**Figure 4c**, **Table S9**) yielded the lowest value of 11 ± 8 % for Brnoteplase-treated rats (2.5 mg/kg), followed by 13 ± 5 % for tenecteplase-treated (0.25 mg/kg) and 15 ± 11 % for alteplase-treated (0.9 mg/kg) groups. The lowest asymmetry in the Brnoteplase group is coupled with the highest overall HT incidence, reflecting the highest recanalization frequency (**Figure S14**), and the predominance of the least dangerous HT grade

683 (HI1). Together with the lowest observed proportion of severe HT (PH1; **Figure 4b**), this
684 outcome indicates that Brnoteplase treatment was associated with reduced brain swelling and
685 infarct expansion compared to the administration of alteplase or tenecteplase, suggesting a
686 potentially more favorable safety profile.

687 **Rat plasma analysis corroborates superior Brnoteplase properties**

688 Rat plasma collected at the end of the thrombolysis effectivity experiments was analyzed to
689 determine circulating levels of plasminogen, plasmin, and the administered thrombolytic (**Figure**
690 **5**, **Table S10**). Residual thrombolytic concentrations provided information about residence time
691 and half-life (**Figure 5a**, **Table S10**). The results yielded 37-, 11-, and 30-fold increased levels
692 of active Brnoteplase over alteplase at doses of 0.9, 2.5, and 5.0 mg/kg, respectively. Notably,
693 the residual active Brnoteplase concentration after administering the 0.9 mg/kg dose (0.22 ±
694 0.06 mg/L) was significantly higher even than the alteplase concentration after 5.0 mg/kg (0.09
695 ± 0.01 mg/L). The distinct administration regimes—bolus for Brnoteplase vs. continuous rate
696 infusion for alteplase—underscore this difference and support that the improved inhibition
697 resistance of Brnoteplase (**Figure 2e**) and potentially alleviated binding to clearance receptors
698 (**Table 3**) substantially extended its biological half-life.

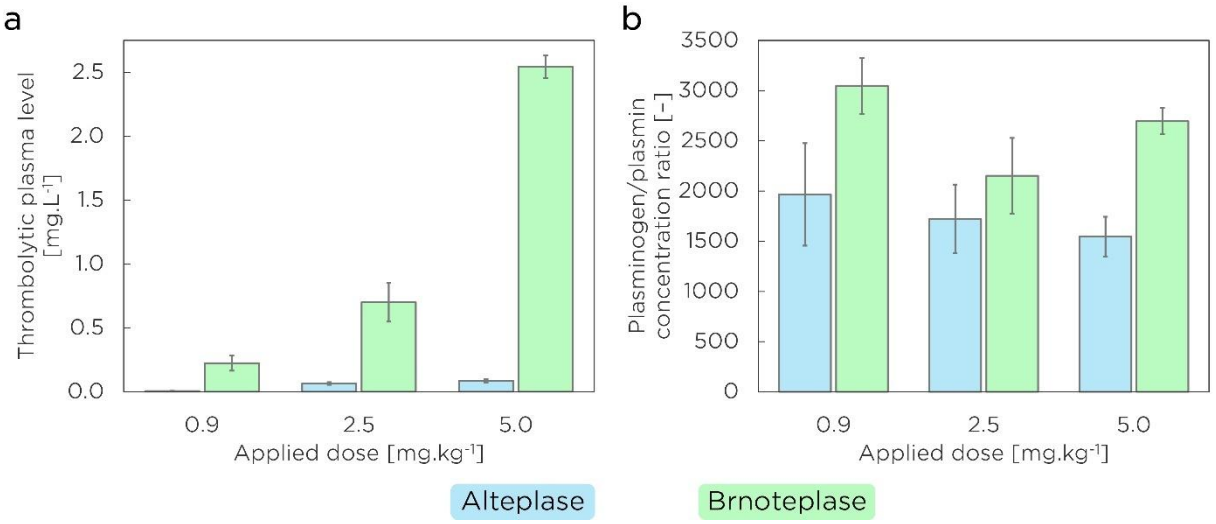

699
700 **Figure 5: Determination of pharmacological marker levels in rat plasma samples collected at the end of the**
701 **thrombolysis effectivity experiments.** (**a**) Comparison of residual active concentrations of administered
702 thrombolytics as an indicator of the protein residence time and biological half-life. (**b**) Comparison of residual
703 plasminogen-to-plasmin ratios as an indicator of thrombolytic selectivity and safety potential. The bars represent
704 mean values and the whiskers correspond to standard errors.

705 Plasminogen and plasmin levels were quantified to evaluate the thrombolytic
706 pharmacological profile. Substantial systemic plasminemia is associated with increased
707 hemorrhagic risk, whereas preserving high plasminogen levels and restricting plasmin generation
708 to occluded areas promises more favorable treatment outcomes[17]. Accordingly, the
709 plasminogen/plasmin ratio serves as an indicator of thrombolytic selectivity and safety potential.
710 Across all tested doses (0.9, 2.5, and 5.0 mg/kg), Brnoteplase-treated rats exhibited a consistent
711 trend of higher plasminogen/plasmin ratios than the alteplase group (**Figure 5b**, **Table S10**).
712 Furthermore, Brnoteplase treatment at the dose of 5.0 mg/kg retained a comparable or even
713 higher ratio (2700 ± 130) relative to the alteplase group at the clinically relevant dose of 0.9
714 mg/kg (1970 ± 510). Together with the significantly increased *in vivo* thrombolytic efficacy of
715 Brnoteplase (**Figure 4a**), these findings corroborate previously observed enhanced selectivity
716 (**Figure 2c**) and favorable safety profile (**Figure 4bc**) of Brnoteplase.

717 ## Discussion

718 In this study, we established a comprehensive protein engineering pipeline integrating *in silico*
719 rational design, biochemical characterization, *in vitro* clot lysis and penetration assays, and *in*
720 *vivo* animal models. This workflow enables initial high-throughput screening of numerous
721 thrombolytic candidates, followed by systematic filtering to prioritize variants for
722 resource-intensive *in vivo* testing. Through this approach, we identified Brnoteplase, a novel
723 thrombolytic with improved pharmacological properties, representing a promising candidate for
724 future clinical evaluation.

725 Biochemical characterization revealed that Brnoteplase exhibited (i) markedly enhanced
726 fibrin selectivity (80-fold higher than alteplase), (ii) superior resistance to PAI-1 inhibition (4-fold
727 higher), and (iii) increased clot penetration potential (4-fold higher). These parameters are
728 critical determinants of safer and more effective thrombolysis and provide a mechanistic basis
729 for the favorable outcomes observed in subsequent *in vitro* and *in vivo* experiments.

730 The pronounced fibrin selectivity of Brnoteplase ensures activation of plasminogen
731 predominantly within occluded regions with fibrin-containing thrombi, while minimizing systemic

732 plasminemia associated with hemorrhagic risk. As a result, Brnoteplase maintains a higher
733 plasminogen/plasmin ratio relative to alteplase, as confirmed by ELISA analysis of rat plasma
734 collected after thrombolysis. Additionally, the *in silico* design of Brnoteplase aimed to reduce
735 affinity for LRP1 and NMDAR which is expected to mitigate off-target central nervous system
736 interactions and thereby further enhance the safety profile[15,16]. All these findings were
737 corroborated *in vivo*, where the Brnoteplase-treated group exhibited a lower proportion of severe
738 hemorrhagic transformations compared to alteplase and tenecteplase.

739 Improved inhibition resistance, another major characteristic of Brnoteplase, aligns with
740 expectations from the rational design phase. This variant incorporates mutations previously
741 shown to reduce interaction with PAI-1, a primary inhibitor of tissue plasminogen activator in
742 human blood. Together with mutations designed to minimize binding to clearance receptors such
743 as LRP1 and mannose receptors, these combined features were intended to modulate protein
744 pharmacokinetics[6,48,49], and this expectation was confirmed *in vivo*. Rat plasma samples collected
745 at the end of thrombolysis experiments revealed significantly higher residual levels of active
746 Brnoteplase compared to alteplase, indicating an extended biological half-life. This enabled
747 efficient bolus administration, a clinically meaningful advantage over alteplase.

748 Finally, superior clot penetration potential of Brnoteplase in biochemical assays was derived
749 from decreased fibrin affinity. This assumption was validated by *in vitro* assays directly
750 monitoring thrombolytics motion through fibrin matrix gels. Compared to alteplase, Brnoteplase
751 exhibited a faster penetration rate and greater distribution within the clot. This facilitates lysis
752 from within the clot rather than relying solely on surface degradation, which is characteristic of
753 conventional thrombolytics. By promoting more uniform and deeper fibrinolysis, Brnoteplase may
754 accelerate recanalization, particularly in large or densely structured thrombi.

755 In addition to these mechanistic advantages, Brnoteplase demonstrated a favorable dose-
756 response profile *in vitro*. Thrombolytic efficacy progressively increased with concentration until
757 plateau, whereas alteplase exhibited an early peak with a decline at elevated doses. Combined
758 with the Brnoteplase selectivity and reduced affinity for receptors, this profile suggests that
759 higher dosing could enhance thrombolytic potency without compromising safety and hemorrhagic

760 complications. Consistent with these findings, *in vivo* experiments in rat models confirmed that
761 Brnoteplase achieved significantly higher thrombolysis rates and recanalization frequency across
762 all tested doses compared to alteplase. Importantly, safety assessments demonstrated the lowest
763 incidence of severe hemorrhagic transformation and minimal hemispheric asymmetry in
764 Brnoteplase-treated animals relative to both alteplase and tenecteplase. Nevertheless, given the
765 low overall occurrence of hemorrhagic events in the tested cohorts, larger-scale studies will be
766 required to confirm statistical significance of the safety study outcome.

767 Considering that Brnoteplase incorporates several mutations originally introduced in
768 tenecteplase, it is not unexpected that they share a similar profile in biochemical testing, namely
769 fibrin selectivity and PAI-1 resistance. However, Brnoteplase additionally exhibited significantly
770 greater fibrin clot penetration and a lower rate of severe hemorrhagic transformation,
771 positioning it as a potentially advantageous alternative within the class of current state-of-the-
772 art thrombolytics.

773 In summary, we developed a comprehensive and scalable workflow for the rational design,
774 rapid initial screening and prioritization, and the final selection of the most viable and clinically
775 relevant novel thrombolytic proteins. By applying this pipeline, we generated Brnoteplase, an
776 alteplase variant combining enhanced fibrin selectivity, improved inhibition resistance,
777 prolonged biological half-life, superior clot penetration, and a favorable dose–response profile.
778 These attributes collectively translate into higher thrombolytic efficacy and a promising safety
779 profile in preclinical *in vivo* models. While further validation in larger animal cohorts is essential,
780 Brnoteplase represents a strong candidate for follow-up (pre)clinical studies. By enabling bolus
781 administration due to extended half-life, reducing hemorrhagic risk via diminished systemic
782 plasminemia, and accelerating recanalization through deeper intrathrombus penetration,
783 Brnoteplase has the potential to advance acute ischemic stroke therapy beyond the limitations
784 of current thrombolytic agents.

Funding

This work was supported by the Czech Ministry of Education (INBIO - CZ.02.1.01/0.0/0.0/16_026/0008451, ENOCH - CZ.02.1.01/0.0/0.0/16_019/0000868); Grant Agency of Czech Republic (20-15915Y); and National Institute for Neurology Research (LX22NPO5107 MEYS) Financed by European Union – Next Generation EU. MT, ST, and JSM are supported by the scholarship Brno Ph.D. Talent and MM is supported by the Masaryk University (MUNI/H/1561/2018). ST, MP, and JV received additional support from the Ministry of Health of the Czech Republic in cooperation with the Czech Health Research Council under project No. NW24-08-00064. Computational resources were provided by the e-INFRA CZ project (ID:90254), supported by the Ministry of Education, Youth and Sports of the Czech Republic, and by the ELIXIR-CZ project (ID:90255), part of the international ELIXIR infrastructure.

Author Contribution Statement.

J.M and D.B. performed the *in silico* analysis and selection of the initial thrombolytic pool. **Pe.Ka. and T.B.** produced the designed thrombolytic enzymes. **M.T. and V.S.** performed the biochemical characterization of selected proteins and ELISA measurements of rat plasma samples and analyzed the corresponding data. **S.T., M.P., Pa.Ki., and J.V.** performed the *in vitro* thrombolysis and fibrin penetration assays and analyzed the corresponding data. **P.S., J.H., E.B., A.D.A., J.B., and J.O.** performed the *in vivo* animal testing and the corresponding data analysis and statistical evaluation. **M.T., V.S.** drafted the initial version of the manuscript with the help of **J.M., S.T., and J. V.**. **J.D., Z.P., D.B., M.M., J.V., L.K., and R.M.** conceived and designed the study, supervised the project, and acquired funding. **All authors** reviewed and interpreted the data, critically revised the manuscript, and approved the final version.

Acknowledgements

We thank the laboratory technicians Marketa Stuchla, Veronika Novakova, Irena Halikova, and Klara Markova for their assistance with the preparation of common reagents and sample storage.

Conflict of Interest

None declared.

References

1. Feigin VL, Brainin M, Norrving B, et al. World Stroke Organization: Global Stroke Fact Sheet 2025. *Int J Stroke*. 2025;20(2):132-144. doi:10.1177/17474930241308142

2. Aguiar de Sousa D, von Martial R, Abilleira S, et al. Access to and delivery of acute ischaemic stroke treatments: A survey of national scientific societies and stroke experts in 44 European countries. *Eur Stroke J*. 2019;4(1):13-28. doi:10.1177/2396987318786023

3. Xiong Y, Wakhloo AK, Fisher M. Advances in Acute Ischemic Stroke Therapy. *Circ Res*. 2022;130(8):1230-1251. doi:10.1161/CIRCRESAHA.121.319948

4. Yaghi S, Willey JZ, Cucchiara B, et al. Treatment and Outcome of Hemorrhagic Transformation After Intravenous Alteplase in Acute Ischemic Stroke: A Scientific Statement for Healthcare Professionals From the American Heart Association/American Stroke Association. *Stroke*. 2017;48(12):e343-e361. doi:10.1161/STR.0000000000000152

5. Mosconi MG, Paciaroni M. Treatments in Ischemic Stroke: Current and Future. *Eur Neurol*. 2022;85(5):349-366. doi:10.1159/000525822

6. Mican J, Toul M, Bednar D, Damborsky J. Structural Biology and Protein Engineering of Thrombolytics. *Comput Struct Biotechnol J*. 2019;17:917-938. doi:10.1016/j.csbj.2019.06.023

7. Potla N, Ganti L. Tenecteplase vs. alteplase for acute ischemic stroke: a systematic review. *Int J Emerg Med*. 2022;15(1):1. doi:10.1186/s12245-021-00399-w

8. Burwell JM, Howay JR, Wasko L, et al. Tenecteplase is here: navigating the shift of a stroke thrombolytic in the United States prior to FDA approval: a mini-review on rationale, barriers, and pathways. *Front Neurol*. 2025;16:1563423. doi:10.3389/fneur.2025.1563423

9. Rodriguez M, Sidebottom C, Wells DA, et al. A Systematic Review of the Efficacy and Safety of Tenecteplase Versus Alteplase in Acute Ischemic Stroke: A Time to Pass the Torch. *Stroke Vasc Interv Neurol*. 2024;4(4):e001110. doi:10.1161/SVIN.123.001110

10. Ma Y, Xiang H, Busse JW, et al. Tenecteplase versus alteplase for acute ischemic stroke: a systematic review and meta-analysis of randomized and non-randomized studies. *J Neurol*. 2024;271(5):2309-2323. doi:10.1007/s00415-024-12243-1

11. Rose D, Cavalier A, Kam W, et al. Complications of Intravenous Tenecteplase Versus Alteplase for the Treatment of Acute Ischemic Stroke: A Systematic Review and Meta-Analysis. *Stroke*. 2023;54(5):1192-1204. doi:10.1161/STROKEAHA.122.042335

12. Warach SJ, Dula AN, Milling TJ. Tenecteplase Thrombolysis for Acute Ischemic Stroke. *Stroke*. 2020;51(11):3440-3451. doi:10.1161/STROKEAHA.120.029749

13. Meng X, Li S, Dai H, et al. Tenecteplase vs Alteplase for Patients With Acute Ischemic Stroke: The ORIGINAL Randomized Clinical Trial. *JAMA*. 2024;332(17):1437-1445. doi:10.1001/jama.2024.14721

848 14. Van de Werf FJ. The ideal fibrinolytic: can drug design improve clinical results? *Eur Heart J*.
849 1999;20(20):1452-1458. doi:10.1053/euhj.1999.1659

850 15. Maier W, Bednorz M, Meister S, et al. LRP1 is critical for the surface distribution and
851 internalization of the NR2B NMDA receptor subtype. *Mol Neurodegener*. 2013;8(1):25.
852 doi:10.1186/1750-1326-8-25

853 16. Baron A, Montagne A, Cassé F, et al. NR2D-containing NMDA receptors mediate tissue
854 plasminogen activator-promoted neuronal excitotoxicity. *Cell Death Differ*. 2010;17(5):860-
855 871. doi:10.1038/cdd.2009.172

856 17. Nikitin D, Choi S, Mican J, et al. Development and Testing of Thrombolytics in Stroke. *J*
857 *Stroke*. 2021;23(1):12-36. doi:10.5853/jos.2020.03349

858 18. Lenka S, Jan S, T M, David B, Jiri D. HotSpot Wizard 3.0: web server for automated design of
859 mutations and smart libraries based on sequence input information. *Nucleic Acids Res*.
860 2018;46(W1):W356-W362. doi:10.1093/nar/gky417

861 19. Alford RF, Leaver-Fay A, Jeliazkov JR, et al. The Rosetta All-Atom Energy Function for
862 Macromolecular Modeling and Design. *J Chem Theory Comput*. 2017;13(6):3031-3048.
863 doi:10.1021/acs.jctc.7b00125

864 20. Prasad JM, Young PA, Strickland DK. High Affinity Binding of the Receptor-associated Protein
865 D1D2 Domains with the Low Density Lipoprotein Receptor-related Protein (LRP1) Involves
866 Bivalent Complex Formation: CRITICAL ROLES OF LYSINES 60 AND 191*. *J Biol Chem*.
867 2016;291(35):18430-18439. doi:10.1074/jbc.M116.744904

868 21. Freeman R, Niego B, R. Croucher D, Pedersen LO, Medcalf RL. t-PA, but not desmoteplase,
869 induces plasmin-dependent opening of a blood-brain barrier model under normoxic and
870 ischaemic conditions. *Brain Res*. 2014;1565:63-73. doi:10.1016/j.brainres.2014.03.027

871 22. M M, Rt K, A B, et al. FireProtASR: A Web Server for Fully Automated Ancestral Sequence
872 Reconstruction. *Brief Bioinform*. 2021;22(4):bbaa337. doi:10.1093/bib/bbaa337

873 23. J H, S B, J S, et al. EnzymeMiner: automated mining of soluble enzymes with diverse
874 structures, catalytic properties and stabilities. *Nucleic Acids Res*. 2020;48(W1):W104-W109.
875 doi:10.1093/nar/gkaa372

876 24. Toschi L, Bringmann P, Petri T, Donner P, Schleuning WD. Fibrin selectivity of the isolated
877 protease domains of tissue-type and vampire bat salivary gland plasminogen activators. *Eur*
878 *J Biochem*. 1998;252(1):108-112. doi:10.1046/j.1432-1327.1998.2520108.x

879 25. Harpaz D, Chen X, Francis CW, Marder VJ, Meltzer RS. Ultrasound enhancement of
880 thrombolysis and reperfusion in vitro. *J Am Coll Cardiol*. 1993;21(6):1507-1511.
881 doi:10.1016/0735-1097(93)90331-T

882 26. Prasad S, Kashyap RS, Deopujari JY, Purohit HJ, Taori GM, Daginawala HF. Development of
883 an in vitro model to study clot lysis activity of thrombolytic drugs. *Thromb J*. 2006;4:14.
884 doi:10.1186/1477-9560-4-14

885 27. Thalerová S, Pešková M, Kittová P, et al. Effect of Apixaban Pretreatment on Alteplase-
886 Induced Thrombolysis: An In Vitro Study. *Front Pharmacol*. 2021;12:740930.
887 doi:10.3389/fphar.2021.740930

888 28. Víteček J, Wünschová AV, Thalerová S, et al. Factors influencing the efficacy of recombinant
889 tissue plasminogen activator: Implications for ischemic stroke treatment. *PLOS ONE*.
890 2024;19(6):e0302269. doi:10.1371/journal.pone.0302269

29. Thalerová S, Wünschová AV, Kittová P, et al. A collateral circulation in ischemic stroke accelerates recanalization due to lower clot compaction. *PLOS ONE*. 2024;19(11):e0314079. doi:10.1371/journal.pone.0314079

30. Nikitin D, Mican J, Toul M, et al. Computer-aided engineering of staphylokinase toward enhanced affinity and selectivity for plasmin. *Comput Struct Biotechnol J*. 2022;20:1366-1377. doi:10.1016/j.csbj.2022.03.004

31. Diamond SL. Engineering Design of Optimal Strategies for Blood Clot Dissolution. *Annu Rev Biomed Eng*. 1999;1(Volume 1, 1999):427-461. doi:10.1146/annurev.bioeng.1.1.427

32. Acheampong P, and Ford GA. Pharmacokinetics of alteplase in the treatment of ischaemic stroke. *Expert Opin Drug Metab Toxicol*. 2012;8(2):271-281. doi:10.1517/17425255.2012.652615

33. Elnager A, Abdullah WZ, Hassan R, et al. In Vitro Whole Blood Clot Lysis for Fibrinolytic Activity Study Using D-Dimer and Confocal Microscopy. *Adv Hematol*. 2014;2014:814684. doi:10.1155/2014/814684

34. Rottenberger Z, Komorowicz E, Szabó L, et al. Lytic and mechanical stability of clots composed of fibrin and blood vessel wall components. *J Thromb Haemost*. 2013;11(3):529-538. doi:10.1111/jth.12112

35. Marcos-Contreras OA, Ganguly K, Yamamoto A, et al. Clot penetration and retention by plasminogen activators promote fibrinolysis. *Biochem Pharmacol*. 2013;85(2):216-222. doi:10.1016/j.bcp.2012.10.011

36. Longstaff C. Measuring fibrinolysis: from research to routine diagnostic assays. *J Thromb Haemost*. 2018;16(4):652-662. doi:10.1111/jth.13957

37. Longstaff C, Varjú I, Sótonyi P, et al. Mechanical Stability and Fibrinolytic Resistance of Clots Containing Fibrin, DNA, and Histones*. *J Biol Chem*. 2013;288(10):6946-6956. doi:10.1074/jbc.M112.404301

38. Morrow GB, Whyte CS, Mutch NJ. Functional plasminogen activator inhibitor 1 is retained on the activated platelet membrane following platelet activation. *Haematologica*. 2019;105(12):2824-2833. doi:10.3324/haematol.2019.230367

39. Vítečková Wünschová A, Novobilský A, Hložková J, et al. Thrombus Imaging Using 3D Printed Middle Cerebral Artery Model and Preclinical Imaging Techniques: Application to Thrombus Targeting and Thrombolytic Studies. *Pharmaceutics*. 2020;12(12):1207. doi:10.3390/pharmaceutics12121207

40. Kavkova M, Zikmund T, Kala A, et al. Contrast enhanced X-ray computed tomography imaging of amyloid plaques in Alzheimer disease rat model on lab based micro CT system. *Sci Rep*. 2021;11(1):5999. doi:10.1038/s41598-021-84579-x

41. Bassel-Duby R, Jiang NY, Bittick T, et al. Tyrosine 67 in the epidermal growth factor-like domain of tissue-type plasminogen activator is important for clearance by a specific hepatic receptor. *J Biol Chem*. 1992;267(14):9668-9677.

42. López-Atalaya JP, Roussel BD, Ali C, et al. Recombinant Desmodus rotundus salivary plasminogen activator crosses the blood-brain barrier through a low-density lipoprotein receptor-related protein-dependent mechanism without exerting neurotoxic effects. *Stroke*. 2007;38(3):1036-1043. doi:10.1161/01.STR.0000258100.04923.84

933 43. Narita M, Bu G, Herz J, Schwartz AL. Two receptor systems are involved in the plasma
934 clearance of tissue-type plasminogen activator (t-PA) in vivo. *J Clin Invest*. 1995;96(2):1164-
935 1168. doi:10.1172/JCI118105

936 44. Goulay R, Naveau M, Gaberel T, Vivien D, Parcq J. Optimized tPA: A non-neurotoxic
937 fibrinolytic agent for the drainage of intracerebral hemorrhages. *J Cereb Blood Flow Metab*.
938 2018;38(7):1180-1189. doi:10.1177/0271678X17719180

939 45. Keyt BA, Paoni NF, Refino CJ, et al. A faster-acting and more potent form of tissue
940 plasminogen activator. *Proc Natl Acad Sci U S A*. 1994;91(9):3670-3674.
941 doi:10.1073/pnas.91.9.3670

942 46. Hacke W, Kaste M, Fieschi C, et al. Randomised double-blind placebo-controlled trial of
943 thrombolytic therapy with intravenous alteplase in acute ischaemic stroke (ECASS II). *The*
944 *Lancet*. 1998;352(9136):1245-1251. doi:10.1016/S0140-6736(98)08020-9

945 47. Ma J, Ma Y, Shuaib A, Winship IR. Improved collateral flow and reduced damage after remote
946 ischemic perconditioning during distal middle cerebral artery occlusion in aged rats. *Sci Rep*.
947 2020;10(1):12392. doi:10.1038/s41598-020-69122-8

948 48. Biessen EAL, van Teijlingen M, Vietsch H, et al. Antagonists of the Mannose Receptor and the
949 LDL Receptor–Related Protein Dramatically Delay the Clearance of Tissue Plasminogen
950 Activator. *Circulation*. 1997;95(1):46-52. doi:10.1161/01.CIR.95.1.46

951 49. Chandler WL, Alessi MC, Aillaud MF, Henderson P, Vague P, Juhan-Vague I. Clearance of
952 Tissue Plasminogen Activator (TPA) and TPA/Plasminogen Activator Inhibitor Type 1 (PAI-1)
953 Complex. *Circulation*. 1997;96(3):761-768. doi:10.1161/01.CIR.96.3.761

954 50. Meiners K, Hamm P, Gutmann M, et al. Site-specific PEGylation of recombinant tissue-type
955 plasminogen activator. *Eur J Pharm Biopharm*. 2023;192:79-87.
956 doi:10.1016/j.ejpb.2023.09.017

957 51. Toul M, Slonkova V, Mican J, et al. Identification, characterization, and engineering of
958 glycosylation in thrombolytics. *Biotechnol Adv*. 2023;66:108174.
959 doi:10.1016/j.biotechadv.2023.108174

960 52. Ma H, Jiang Z, Xu J, Liu J, Guo ZN. Targeted nano-delivery strategies for facilitating
961 thrombolysis treatment in ischemic stroke. *Drug Deliv*. 28(1):357-371.
962 doi:10.1080/10717544.2021.1879315

963 53. Zenych A, Fournier L, Chauvierre C. Nanomedicine progress in thrombolytic therapy.
964 *Biomaterials*. 2020;258:120297. doi:10.1016/j.biomaterials.2020.120297

965 54. Rijken DC, Barrett-Bergshoeff MM, Jie AFH, Criscuoli M, Sakharov DV. Clot penetration and
966 fibrin binding of amediplase, a chimeric plasminogen activator (K2tu-PA). *Thromb Haemost*.
967 2017;91:52-60. doi:10.1160/TH03-07-0435

968 55. Tsikouris JP, White CM. Tenecteplase - A novel fibrin-specific thrombolytic agent for
969 treatment of acute myocardial infarction. *Formulary*. 2000;35(8):647-653.

970 56. Tanswell P, Modi N, Combs D, Danays T. Pharmacokinetics and pharmacodynamics of
971 tenecteplase in fibrinolytic therapy of acute myocardial infarction. *Clin Pharmacokinet*.
972 2002;41(15):1229-1245. doi:10.2165/00003088-200241150-00001

973 57. Logallo N, Novotny V, Assmus J, et al. Tenecteplase versus alteplase for management of
974 acute ischaemic stroke (NOR-TEST): a phase 3, randomised, open-label, blinded endpoint
975 trial. *Lancet Neurol*. 2017;16(10):781-788. doi:10.1016/S1474-4422(17)30253-3

976 58. Campbell BCV, Mitchell PJ, Churilov L, et al. Tenecteplase versus Alteplase before
977 Thrombectomy for Ischemic Stroke. *N Engl J Med*. Published online 2018:10.

978 59. Huang J, Zheng H, Zhu X, Zhang K, Ping X. Tenecteplase versus alteplase for the treatment
979 of acute ischemic stroke: a meta-analysis of randomized controlled trials. *Ann Med*.
980 56(1):2320285. doi:10.1080/07853890.2024.2320285

981 60. Xu Y, Chen D, Liu P, et al. A triple fusion tissue-type plasminogen activator (TriF-ΔtPA)
982 enhanced thrombolysis in carotid embolism-induced stroke model. *Int J Pharm*.
983 2023;637:122878. doi:10.1016/j.ijpharm.2023.122878

984 61. Chen S, Fang S, Zhou Y, et al. A low bleeding risk thrombolytic agent: citPA5. *Cardiovasc*
985 *Res*. 2024;120(10):cvae060. doi:10.1093/cvr/cvae060

986